Original Article

Possibility of re-purposing antifungal drugs posaconazole & isavuconazole against promastigote form of Leishmania major

Chandra Kanta Bhusal[1,3], Pooja Beniwal[2], Sarman Singh[1], Davinder Kaur[3], Upninder Kaur[3], Sukhbir Kaur[2] & Rakesh Sehgal[1,3]

[1]Department of Microbiology, Aarupadai Veedu Medical College & Hospital, Puducherry, [2]Department of Zoology, Panjab University, & [3]Department of Medical Parasitology, Post Graduate Institute of Medical Education and Research, Chandigarh, Punjab, India

Background & objectives: The emergence of drug resistance in leishmaniasis has remained a concern. Even new drugs have been found to be less effective within a few years of their use. Coupled with their related side effects and cost-effectiveness, this has prompted the search for alternative therapeutic options. In this study, the Computer Aided Drug Design (CADD) approach was used to repurpose already existing drugs against *Leishmania major*. The enzyme lanosterol 14-alpha demethylase (CYP51), in *L. major*, was chosen as the drug target since it is a key enzyme involved in synthesizing ergosterol, a crucial component of the cell membrane.

Methods: A library of 1615 FDA-approved drugs was virtually screened and docked with modeled CYP51 at its predicted binding site. The drugs with high scores and high affinity were subjected to Molecular Dynamics (MD) simulations for 100 ns. Finally, the compounds were tested *in vitro* using an MTT [3-(4,5-Dimethylthiazol-2-yl)-2,5-Diphenyltetrazolium Bromide] assay against the promastigotes of *L. major*.

Results: Computational screening of FDA-approved drugs identified posaconazole and isavuconazole as promising candidates, as both drugs target the CYP51 enzyme in fungi. Molecular dynamics (MD) simulations demonstrated that both drugs form stable complexes with the target enzyme. *In vitro* studies of posaconazole and isavuconazole against promastigotes of *L. major* demonstrated significant efficacy, with IC_{50} values of 2.062±0.89 μg/ml and 1.202±0.47 μg/ml, respectively.

Interpretation & conclusions: The study showed that the existing FDA-approved drugs posaconazole and isavuconazole can successfully be repurposed for treating *L. major* by targeting the CYP51 enzyme, demonstrating significant efficacy against promastigotes.

Leishmaniasis is a disease caused by protozoan parasites from more than 20 different Leishmania species. It presents in three primary forms: visceral leishmaniasis (VL), cutaneous leishmaniasis (CL), and mucocutaneous leishmaniasis[1,2]. VL, the most severe form, is fatal if untreated in over 95 per cent

of cases and is characterized by symptoms like fever, weight loss, and organ enlargement. It primarily affects regions such as Brazil, East Africa, and India[3,4]. CL causes skin ulcers and is prevalent in the Americas, the Mediterranean basin, the Middle East, and Central Asia. Mucocutaneous leishmaniasis leads to the destruction of mucous membranes in the nose, mouth, and throat, with most cases found in Bolivia, Brazil, Ethiopia, and Peru[5,6]. Leishmaniasis disproportionately affects the world's poorest populations, associated with factors like malnutrition, poor housing, and weakened immune systems. Despite an estimated 700,000 to 1 million new cases annually, only a small fraction develops symptoms. The disease's epidemiology varies by region, with different forms and species prevalence across Africa, the Americas, the Eastern Mediterranean, Europe, and South-East Asia[7].

Leishmania has developed resistance to key drugs like antimony, miltefosine, and amphotericin B, complicating treatment efforts. Antimony resistance in Leishmania is primarily due to reduced drug uptake facilitated by the downregulation of aquaglyceroporin 1 (AQP1) and increased intracellular thiol levels, which enhance the parasite's antioxidant capacity. Additionally, increased drug efflux through ATP-binding cassette (ABC) transporters and modulation of host immune responses contribute to resistance[8,9]. Miltefosine resistance involves decreased drug accumulation, overexpression of multidrug resistance proteins like MRPA, and genetic mutations affecting lipid metabolism and transporter activity. These mechanisms are often stable and specific to miltefosine, with some strains also showing cross-resistance to other drugs[10-12]. Amphotericin B (AmB) resistance is associated with mutations in the sterol biosynthesis pathway, leading to altered membrane sterol composition and decreased drug binding affinity. This resistance can result from both laboratory-induced mutations and natural selection in clinical settings[13-15]. The complexity and persistence of these resistance mechanisms highlight the urgent need for new therapeutic approaches, including novel drugs and drug combinations, to effectively treat resistant strains of Leishmania.

A lot of drug targets have been explored in leishmania to seek new therapeutic opportunities. Squalene epoxidase, 3-hydroxy-3-methyl-glutaryl-CoA reductase (HMGR) enzyme from sterol biosynthetic pathway[16,17], glyceraldehyde-3-phosphate dehydrogenase (GAPDH) and phosphoglycerate kinase from glycolytic pathway[18], dihydrofolate reductase (DHFR) and pteridine reductase 1(PTR1) from folate biosynthesis pathway[19,20], trypanthione reductase from trypanothione pathway[21], spermidine synthase from hypusine pathway[22], L-asparaginase[23] *etc*., have been extensively studied as their potency as drug targets. Lanosterol 14-alpha demethylase from the sterol biosynthetic pathway in Leishmania is a promising candidate due to its crucial role in sterol biosynthesis, which is essential for maintaining the parasite's cell membrane integrity. Lanosterol 14-alpha demethylase (CYP51) is an attractive drug target in Leishmania as it has a unique role in ergosterol biosynthesis, a pathway absent in humans that minimizes off-target effects and enhances safety. This specificity allows for a broader therapeutic window, potentially enabling higher doses without host toxicity. The extensive research on CYP51 in fungi provides valuable insights into drug development, resistance mechanisms, and pharmacokinetics, facilitating the design of effective inhibitors. Additionally, the fitness cost associated with resistance mutations in CYP51 may limit the spread of resistant strains, offering a significant advantage over other targets where resistance can develop more readily[24,25].

Repurposing the existing drugs stands out as a viable solution due to its efficiency in terms of time, ease, and cost-effectiveness. Hence, this research focuses on repurposing FDA-approved drugs against *L. major* through virtual screening and molecular docking. Molecular Dynamics (MD) simulation studies were conducted to study the behaviour and stability of the selected drugs with CYP51 over a span of 100 ns. Finally, an *in vitro* test was conducted to assess the effectiveness of the selected drugs against the survival of the promastigote form of the parasite.

Materials & Methods

The study was conducted at the department of Medical Parasitology, Post Graduate Institute of Medical Education and Research, Chandigarh, Punjab, India from December 2021 to January 2023.

Structural preparation of protein: The amino acid sequence of CYP51 protein from *Leishmania major*, strain Friedlin was retrieved from the NCBI Database[26]. Since the three-dimensional structure of this protein was not available in the Protein Data Bank[27] or UniProt[28], a homology model was generated using the SWISS Model server[29]. To ensure the accuracy

of the modeled structure, validation was conducted using the Structural Analysis and Verification Server (SAVES) version 6.0 (*https://saves.mbi.ucla.edu/*). Using SAVES, ERRAT (*https://www.doe-mbi.ucla.edu/errat/*) was employed to evaluate the quality of the structure, and PROCHECK (*https://www.ebi.ac.uk/thornton-srv/software/PROCHECK/*) was used to plot the Ramachandran plot of the modeled protein[30]. After the structural analysis, the protein was subjected to preprocessing using Discovery Studio (*https://www.3ds.com/products/biovia/discovery-studio*) to optimize the protein structure for precise virtual screening and docking experiments. This involved fixing misoriented groups, creating missing disulfide bonds, removing heteroatoms, deleting water molecules, and adding hydrogen atoms[31].

Prediction of the binding site of proteins: To predict the binding site of the modelled protein, multiple computational tools were employed, including Prankweb[32], ProBIS[33], COACH[34], and Discovery Studio[31]. Each of these tools provided a distinct method for identifying potential binding sites on the protein's surface, allowing for a thorough and comprehensive analysis. After running the protein through each software, the binding sites were individually identified and carefully compared. From this comparative analysis, a consensus sequence was derived, representing the common binding sites predicted by all four tools. This consensus sequence was then utilized to define and generate a grid box, which was essential for conducting accurate virtual screening and molecular docking studies.

Creation of drug library and preparation of the ligands: A drug library containing 1,615 FDA-approved drugs was compiled from the ZINC database[35]. Each drug was validated for FDA approval, and duplicates or invalid entries were removed. The library was then preprocessed using Open Babel, which involved converting molecular formats, generating multiple conformations, assigning charges, and adding hydrogen atoms to the ligands[36]. These steps ensured that the drug library was optimized for accurate virtual screening and molecular docking experiments.

Virtual screening and molecular docking: PyRx 0.8 software (*https://pyrx.sourceforge.io/*) was used to conduct virtual screening and molecular docking, an effective method for identifying potential drug compounds during the drug discovery process[37]. The

drug library, derived from the ZINC database, was initially in .sdf format and contained all the compounds in a single file. To prepare the file for analysis in PyRx 0.8, it was imported from Open Babel. Afterwards, the energy of the ligands was minimized, and all the ligands were converted into AutoDock PDBQT format for further analysis.

On the other hand, the modeled protein was imported into PyRx 0.8. Its energy was minimized, and the protein was converted into. PDBQT format. Subsequently, a grid box was generated by using the binding sequence of CYP51. The dimensions of the grid box were as follows: center (X,Y,Z: 32.50, -27.004, 0.5782) and size (X,Y,Z: 29.089, 28.917, 30.276) with an exhaustiveness of 8. Using PyRx 0.8 and AutoDock Vina, CYP51 was docked within the grid box along with the drug library to study their interactions. The ligands that showed the highest binding energy score and formed a significant number of hydrogen bonds with CYP51 were selected for further analysis. The selected complex docking result was further validated through Autodock 4[38].

Molecular dynamics (MD) simulation and trajectory analysis: The selected protein-ligand complexes from virtual screening were analyzed for molecular dynamic simulation to evaluate their stability. The stability assessment was performed using the Desmond v5.6 module of Schrödinger-Maestro v11.8 in a Linux environment[39]. The simulations were conducted for a period of 100 nanoseconds, employing the Optimized Potentials for Liquid Simulations (OPLS) force field. The simulations were executed at a temperature of 300 Kelvin, following normal pressure and temperature (NPT) conditions.

Trajectory analysis of the molecular dynamics (MD) simulation was used to evaluate structural deviation using Root Mean Square Deviation (RMSD), atomic fluctuations with Root Mean Square Fluctuation (RMSF), and protein-ligand interactions through Protein-Ligand (PL) contacts[39,40].

Antileishmanial Potential of posaconazole and isavuconazole against promastigote: The promastigotes of MHOM/SU/73/5ASKH strain of *Leishmania major* were cultured in RPMI-1640 medium supplemented with 10 per cent FBS and antibiotics (gentamycin and streptomycin) at an ambient temperature (22±1° C) in a biochemical oxygen demand (BOD) incubator. The growing culture was sub-cultured every 48-72h in fresh medium. The effectiveness of posaconazole
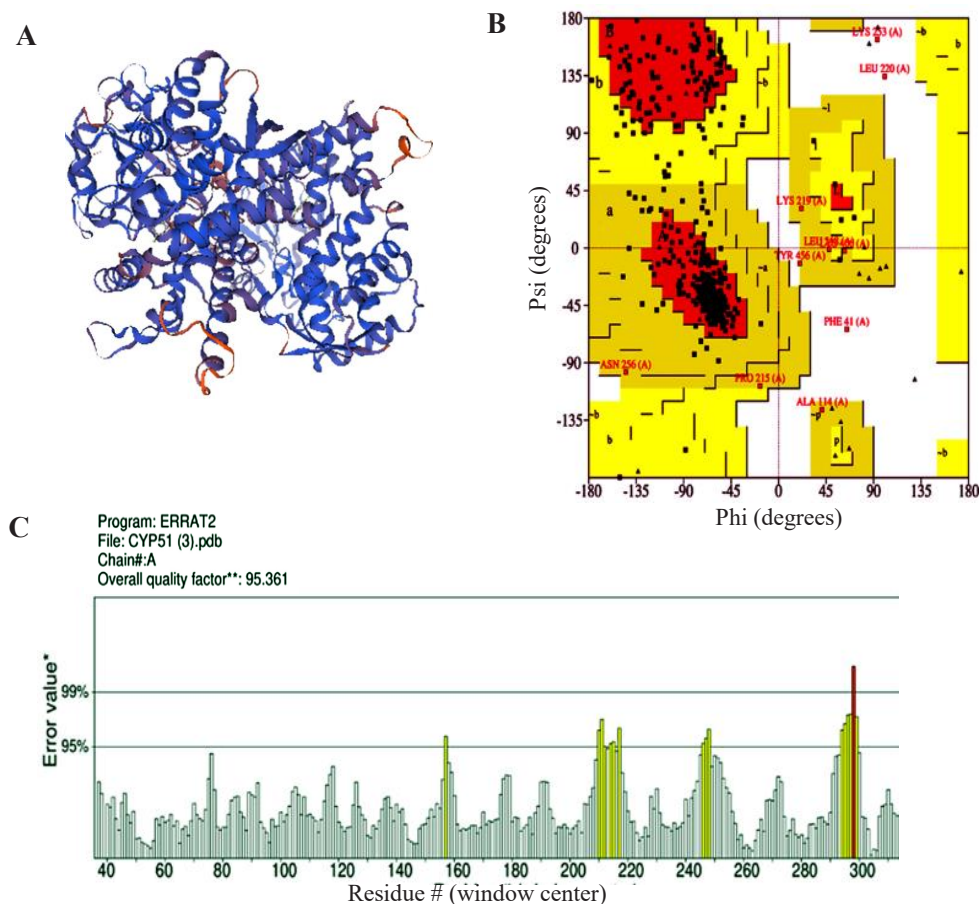
A

B

C

Program: ERRAT2
File: CYP51 (3).pdb
Chain#:A
Overall quality factor**: 95.361

Fig. 1. CYP51 (**A**) 3D model, (**B**) Ramachandran plot and (**C**) ERRAT value.

and isavuconazole against the promastigote stage of *L. major* was assessed using the MTT cell viability assay[41]. Promastigotes, with a cell density of 2×10^5 cells/ml, were cultured with varying concentrations (ranging from 0 to 50 μg/ml) of the test drugs in a BOD incubator for 72h at 24°C. This incubation took place in a 96-well tissue culture plate. Paromomycin was used as a control. The inhibitory concentration of the test drugs (IC_{50}) was determined through extrapolation on a graph (using GraphPad Prism 9.0). The experiments were performed in triplicates and repeated three times.

Results

Modeling and validation of 3D structure of CYP51: The PSI-BLAST algorithm utilized by the Swiss Model was employed to model the 3D structures of CYP51 using the closest homologous protein structures as templates (Fig. 1; panel A). GMQE value on a scale of 0 to 1, served as an indicator of the quality of modeled structure, with scores exceeding 0.8 suggesting high quality (Table I). Over 90 per cent of residues in

all modeled structures resided in the most favored regions of the Ramachandran plot, affirming overall high quality (Fig. 1B). Additionally, ERRAT values, assessing protein structure quality *via* electron density agreement, were above 90, indicating high quality (Fig. 1C). The modeled PDB structure was then imported into Discovery Studio for preprocessing, following the outlined methodology and then saved in .pdb format.

Binding sites of the protein: The binding sites of the CYP51 protein were identified using Prankweb, ProBIS, COACH, and Discovery Studio. Each tool provided unique predictions based on different algorithms, such as deep learning, structural comparison, and integration of multiple scoring functions. The results from these tools were then compared, and a consensus sequence of binding sites was derived from overlapping predictions (Table II). This consensus sequence was used to define the grid box for molecular docking, ensuring that all potential binding regions were accurately targeted in subsequent studies.

Table I. Model assessment metrices

| Putative drug target	Template	GMQE	ERRAT value	Residues in most favored region (Ramachandran plot)
CYP51	3l4d.1.A	0.85	95.10	94%

Table II. Tools and their corresponding binding site sequences for lanosterol 14-alpha-demethylase enzyme (CYP51)

Tools	Binding site sequences
PrankWeb	45, 48,49, 52, 56, 69, 71, 76, 89, 102, 104, 105, 109, 114, 115, 126, 123, 133, 178, 182, 209, 210, 213, 226, 233, 283, 286, 287, 288, 289, 290, 291, 292, 294, 295, 298, 349, 354, 355, 356, 357, 358, 359, 360, 415, 416, 417, 420, 421, 422, 423, 424, 427, 428, 432, 456, 458, 459, 460
ProBIS	102, 115, 123, 126, 129, 133, 287, 290, 291, 294, 349, 354, 355, 358, 360, 415, 420, 421, 422, 423, 427
COACH	9, 114, 122, 126, 133, 287, 290, 291, 294, 295, 298, , 349, 354, 355, 358, 360, 383, 414, 415, 416, 417, 420, 422, 423, 424, 428
Discovery studio	102, 115, 123, 126, 129, 133, 287, 290, 291, 294, 349, 354, 355, 358, 360, 415, 420, 421, 422, 423, 427
Consensus sequence	126, 133, 287, 291, 294, 349, 354, 355, 358, 360, 415, 420, 422, 423

Table III. Selected hit compounds based on binding energy scores, hydrogen bonds and literature review

Ligand	Binding energy (Kcal/mol)	Number of hydrogen bonds	Binding amino acid residues throgh hydrogen bonds
Posaconazole	-10.8	5	TYR 115, HIS 420, LYS 421, CYS 422, TYR 456
Isavuconazole	-9.3	3	TYR 115 (two H-bonds), LYS 421
Fluconazole (control)	-7.1	4	HIS 420 (two H-bonds), ARG 360, TYR 115

TYR, tyrosine; HIS, histidine; ARG, arginine; CYS, cysteine; LYS, lysine
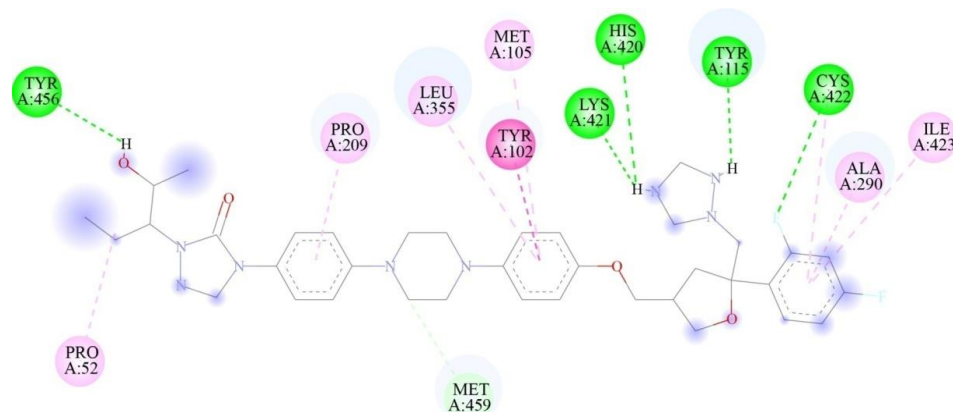
Fig. 2. Two-dimensional representation of binding interactions of posaconazole with the CYP51 protein of *L. major*: conventional H-bonds (green), carbon H-bonds (light green), alkyl (pink), Pi-alkyl (purple), and Pi Pi stacking (magenta) interactions.

Virtual screening and molecular docking of CYP51: Virtual screening and molecular docking analysis were conducted on CYP51 using a library of FDA-approved drugs. The docking results were evaluated based on binding energies and the number of interactions, particularly hydrogen bonds, with key residues of CYP51, with fluconazole used as a target-specific control compound due to its established role in inhibiting CYP51 in fungi (Table III). A threshold was set for binding energies at or below -9 kcal/mol and a minimum of three hydrogen bonds. Posaconazole (Fig. 2) and isavuconazole (Fig. 3) were identified as top candidates due to their strong binding affinities and similar mechanisms of action targeting CYP51 in fungi, making them promising for further study. The docking results of the selected
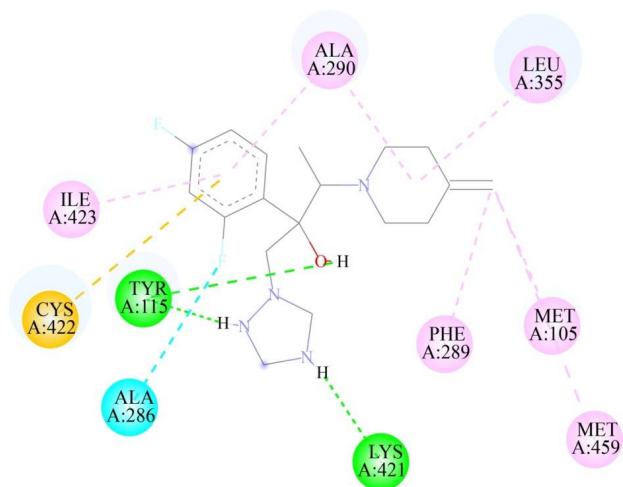
Fig. 3. Two-dimensional representation of binding interactions of isavuconazole with the CYP51 protein of *L. major*: green (H-bond interaction), light green (Carbon hydrogen interaction, cyan (Halogen interaction), orange (Pi-Sulfur interaction), purple (Alkyl interaction), pink (Pi-Alkyl interaction).

Fig. 4. Two-dimensional representation of binding interactions of fluconazole with the CYP51 protein of *L. major*: green (conventional H-bond interaction), light green (Pi-Donor H-bond interaction), and purple (Pi Sigma interaction).

drug-protein complexes were further validated using AutoDock4, where the binding free energies of posaconazole, isavuconazole and fluconazole were found to be -3.54 kcal/mol, -6.03 kcal/mol and -5.58Kcal/mol, respectively. It is important to note that while fluconazole was used as a control for the *in silico* analysis (Fig. 4), in the *in vitro* studies, paromomycin was chosen as the control compound, as it is the standard drug used for killing Leishmania parasites. This distinction reflects the different objectives of the *in silico* and *in vitro* analyses. This common mechanism of action makes them promising candidates for MD simulation and *in vitro* anti-parasitic assessments.

Trajectories of molecular dynamic (MD) simulations: The 100 ns simulation revealed stable conformations for the CYP51 bound to posaconazole and isavuconazole, with Cα-backbone RMSD values ranging from 1.6 to 3.8 A (Fig. 5). The posaconazole- CYP51 complex remained stable, exhibiting minor fluctuations and a low RMSD value. However, between 70 ns and 100 ns, the complex underwent moderate conformational changes, becoming more flexible. The trajectory plot of the isavuconazole- CYP51 complex indicated an initial movement together for the first 10 ns, followed by separation, with the ligand's plot running below the protein's plot. This suggested that the ligand may experience significant conformational changes or explore a different binding site region than the protein.
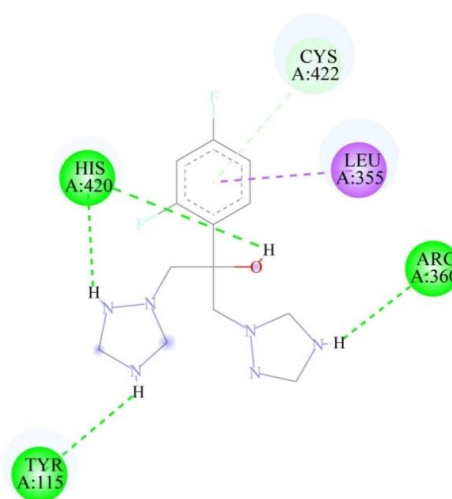
In contrast, the CYP51 protein showed a stable conformation throughout most of the simulation period when complexed with the control drug fluconazole. RMSF study revealed protein dynamics during drug binding. In MD simulations of posaconazole- CYP51 and isavuconazole- CYP51 complexes, the protein mostly maintained stable and rigid conformations (RMSF values <3), with select residues showing higher RMSF values up to 4.5, suggesting increased flexibility in regions like loops or binding sites undergoing conformational changes. Similarly, the control complex, fluconazole-CYP51, showed an overall stable conformation, with some regions displaying flexibility, likely corresponding to loops or binding regions interacting with the drug (Fig. 6).

In posaconazole-CYP51 simulations, significant interactions occurred, with CYS 422 and ARG 360 forming hydrogen bonds 43 per cent and 18 per cent of the time, respectively. Hydrophobic interactions engaged multiple residues for over 50 per cent of the simulation, and occasional water bridges were observed. Similarly, in isavuconazole-CYP51 simulations, stable interactions were noted, with ARG 114 and HIS 420 forming hydrogen bonds with the ligand for approximately 25 per cent and 40 per cent of the simulation, respectively. Hydrophobic interactions involved 11 residues, while no ionic interactions were evident. In contrast, fluconazole-CYP51 simulations revealed stronger hydrogen bonding interactions, with HIS 420, CYS 422, ILE 423, and TYR 115 forming
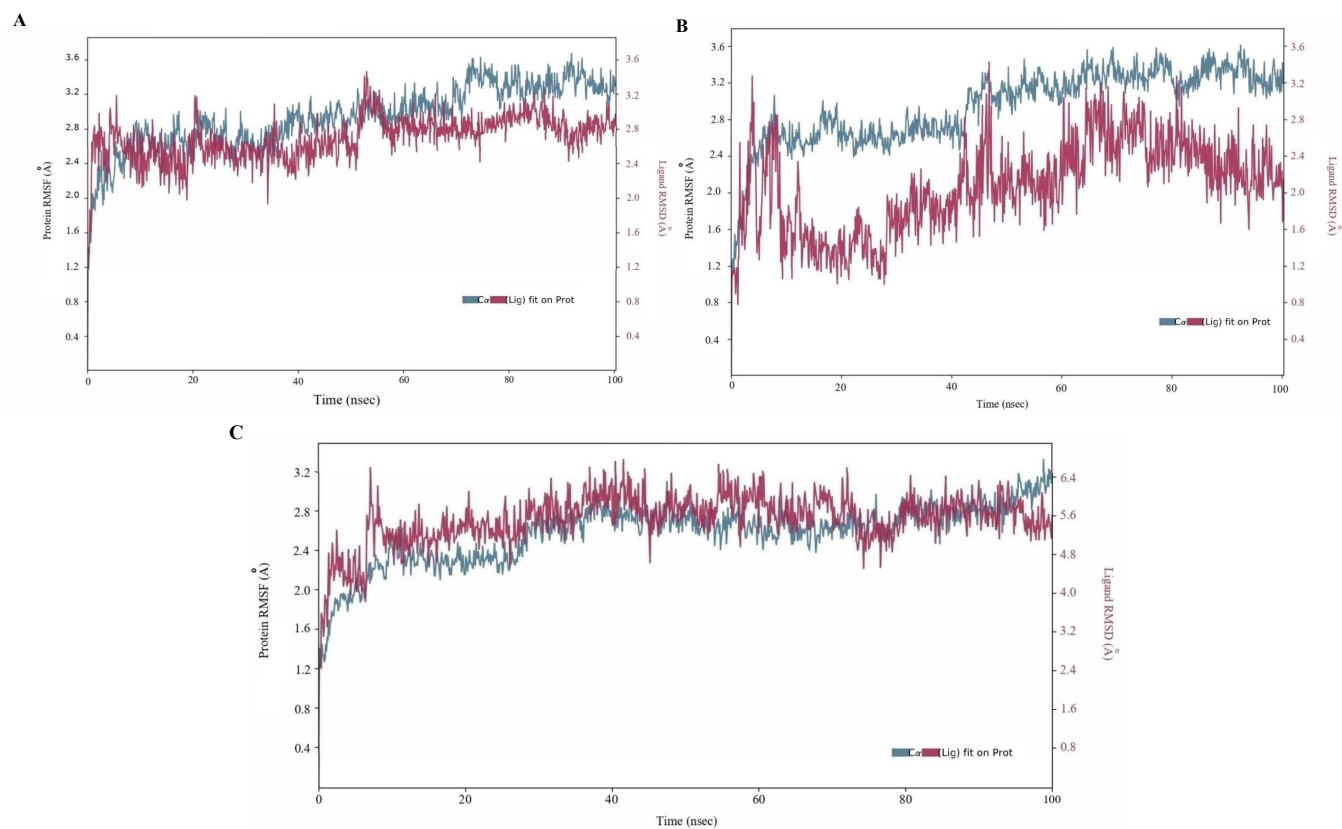
Fig. 5. MD simulation analysis of 100 ns trajectories of Cα-backbone backbone RMSD of CYP51 with (**A**) posaconazole, (**B**) isavuconazole and (**C**) fluconazole.
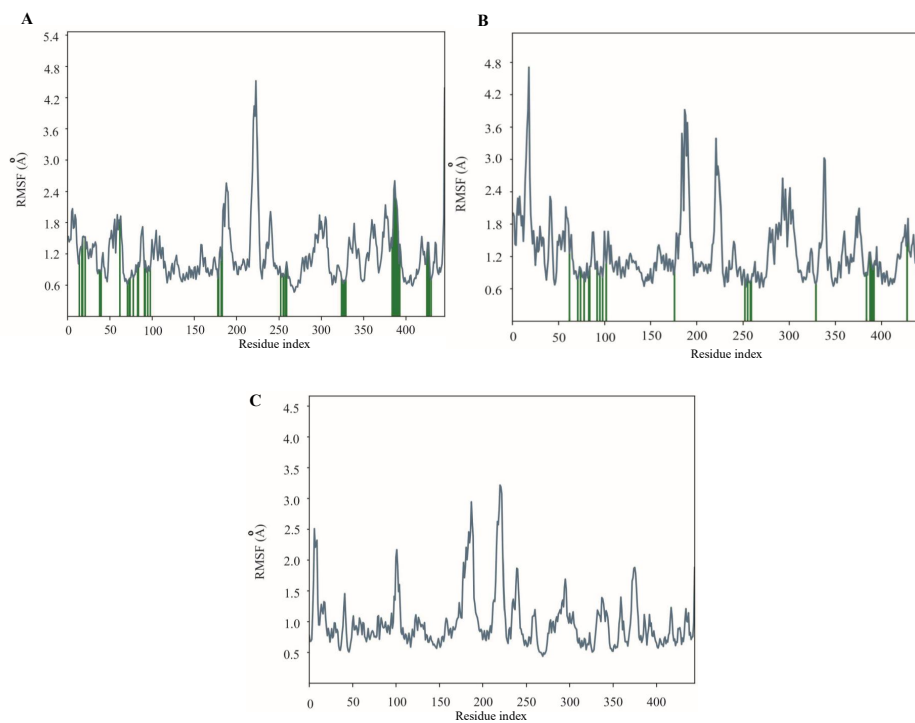

Fig. 6. MD simulation analysis of 100 ns trajectories of RMSF for CYP51 when complexed with (**A**) posaconazole, (**B**) isavuconazole, and (**C**) fluconazole.
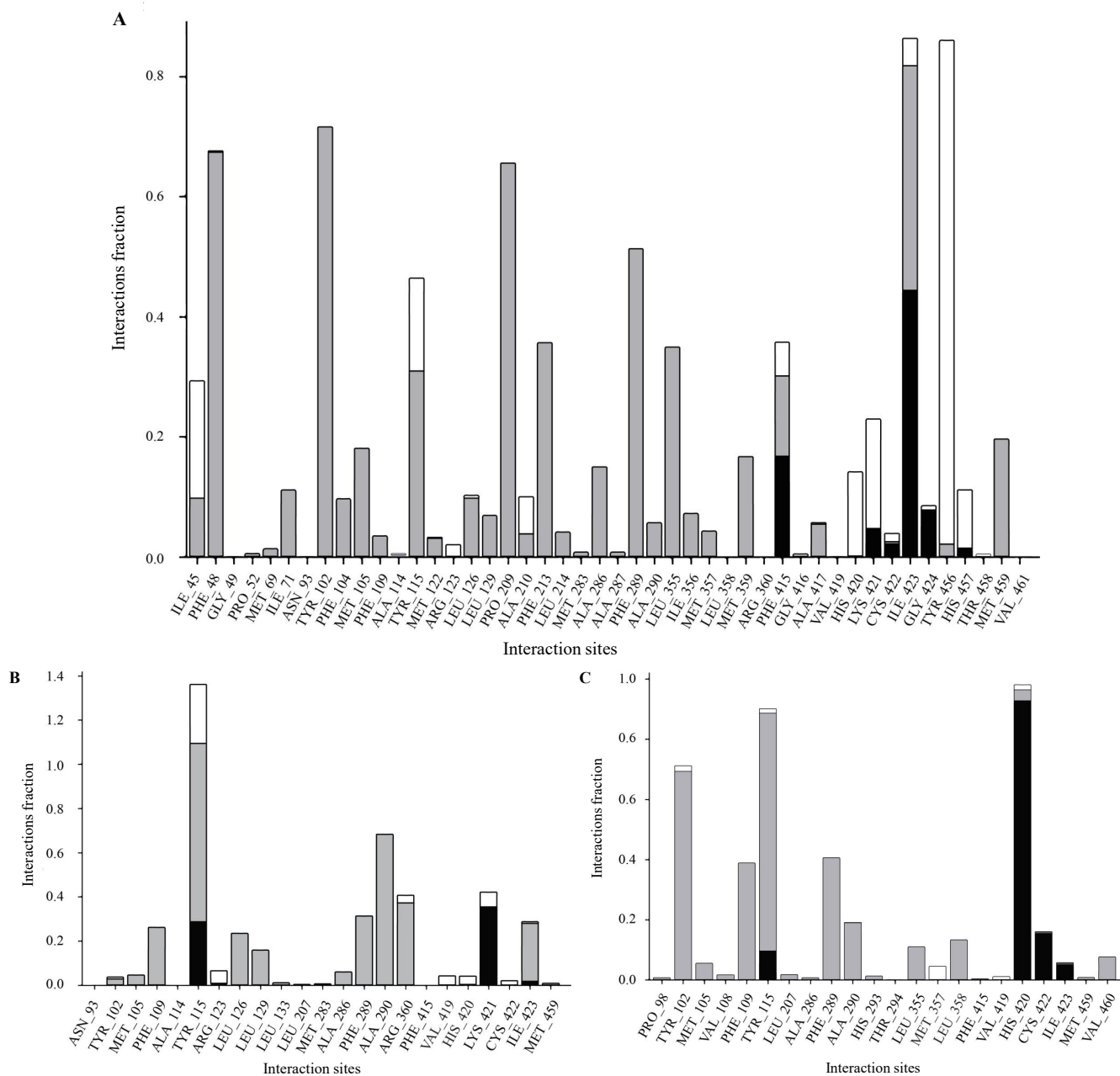
Fig. 7. Protein-Ligand contact for CYP51 with (**A**) posaconazole, (**B**) isavuconazol, and (**C**) fluconazole with grey bars representing hydrophobic interactions, black for hydrogen bonds, and white for water bridges.

H-bonds with fluconazole for approximately 95, 18, 10, and 4 per cent of the simulation period, respectively. Additionally, 17 amino acid residues were involved in hydrophobic interactions with the control drug. Water bridges were observed for a small fraction of the simulation. Compared to the control, both posaconazole and isavuconazole formed fewer hydrogen bonds. Still, they exhibited a wider range of hydrophobic interactions, suggesting potential differences in the stability and flexibility of the complexes (Fig. 7).

Evaluation of antileishmanial activity of posaconazole and isavuconazole in L. major promastigotes through IC$_{50}$: The antileishmanial effect of posaconazole and isavuconazole against exponentially grown *L. major* (strain MHOM/SU/73/5ASKH) promastigotes was examined by an MTT assay. Treatment with posaconazole and isavuconazole (0-150 μg/ml) showed a reduction in parasite growth after 72h of incubation. The IC$_{50}$ values for posaconazole and isavuconazole were calculated with 95 per cent confidence interval,
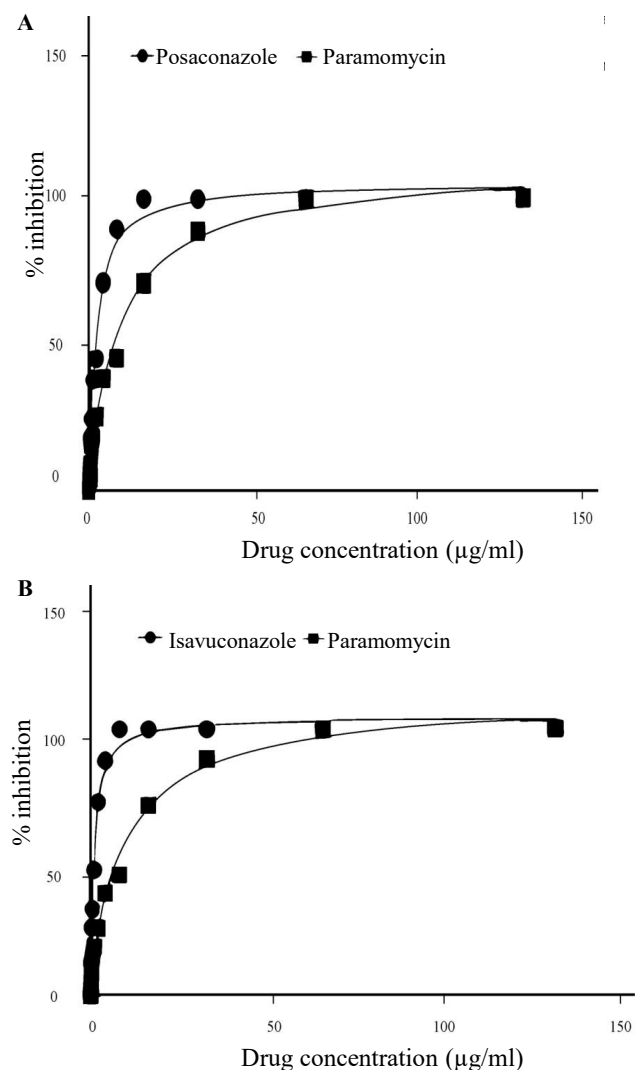
Fig. 8. Dose-response curves showing per cent inhibition of Leishmania growth: (**A**) Posaconazole *vs*. Paromomycin, (**B**) Isavuconazole *vs*. Paromomycin.

yielding 2.062±0.89 µg/ml and 1.202±0.65 µg/ml, respectively indicating their potency in inhibiting the growth of promastigotes. The positive control drug, paromomycin, exhibited an IC_{50} value of 9.420±2.04 µg/ml. These findings demonstrate that both test drugs were effective in inhibiting the growth of *L. major* promastigotes, with isavuconazole showing slightly greater potency.

Discussion

Cutaneous Leishmaniasis (CL) poses a significant public health threat in regions like South America, the Middle East, Central Asia, and parts of Africa, where poverty and limited healthcare exacerbate its spread *via* sandfly bites[42]. Currently, treating cutaneous leishmaniasis has been challenging, with limited options available. Chemotherapy using drugs such as antimonials, paromomycin, miltefosine, and liposomal amphotericin B has been the mainstay, despite their drawbacks including toxicity profiles, potentially higher cost and the emergence of drug resistance[43]. Given these limitations, there is a critical need for innovative therapeutic strategies to address cutaneous leishmaniasis effectively. Hence, in this study, we tried to repurpose FDA-approved drugs against the CYP51 enzyme of *L. major* with the help of virtual screening and molecular docking complemented by MD simulations to validate the findings. Additionally, an *in vitro* study was conducted to assess the efficacy of the selected drugs against the parasite survival.

The enzyme CYP51 was targeted, which plays a pivotal role in *L. major* growth by facilitating the formation of membrane components. While the critical role of CYP51 for parasite survival in *L. major* remains debatable, research by McCall *et al*[44] in 2015, employing gene knockout and pharmacological inhibition experiments, has demonstrated its indispensable role in the closely related species *L. donovani*. Another study by Xu *et al*[45] in 2014 proposed that while CYP51 might not be vital for *L. major*'s survival, its deficiency incurs a substantial fitness penalty, suggesting its essentiality and pivotal role in the parasite's biology and pathogenicity. The lesser similarity of this enzyme with the human proteome also makes it more suitable for use as a drug target, as off-target effects can be avoided.

From a collection of 1615 FDA-approved drugs screened against the modeled CYP51 enzyme, posaconazole (-10.8 kcal/mol with 5 hydrogen bonds) and isavuconazole (-9.3 kcal/mol with 3 hydrogen bonds) exhibited high binding energies and favourable interactions. Recognized for their efficacy against the fungal enzyme CYP51 and sharing approximately 30 per cent similarity with it, posaconazole and isavuconazole were selected for further molecular dynamics (MD) simulations.

In 100 nano second simulations, both CYP51 complexes with posaconazole and isavuconazole initially exhibited stable conformations but demonstrated moderate conformational changes towards the end. The RMSF plots for both posaconazole and isavuconazole show elevated RMSF values in specific regions, suggesting that these areas may correspond to the proteins' loop regions or terminal ends, which are typically more flexible. The MD simulations confirmed the protein-ligand contacts identified in the docking studies, validating the binding residues for the respective drugs as predicted. These

Table IV. Comparison of binding residues for CYP51 complexes with posaconazole and isavuconazole as identified by molecular docking and molecular dynamics simulations

Parameters	Residues		
Binding site predicted	LEU_126, LEU_133, ALA_287, GLY_291, THR_294, ILE_349, PRO_354, LEU_355, LEU_358, ARG_360, PHE_415, HIS_420, CYS_422, ILE_423		
Parameters	Posaconazole	Isavuconazole	Fluconazole
Molecular docking	PRO_52, TYR_102, MET_105, TYR_115, PRO_209, ALA_290, LEU_355, HIS_420, LYS_421, CYS_422, ILE_423, TYR_456, MET_459	MET_105, TYR_115, ALA_286, PHE_289, ALA_290, LEU_355, LYS_421, CYS_422, ILE_423, MET_459	TYR_115, LEU_355, ARG_360, HIS_420, CYS_422
Molecular dynamic simulations	ILE_45, PHE_48, GLY_49, PRO_52, MET_69, ILE_71, ASN_93, TYR_102, PHE_104, MET_105, PHE_109, ALA_114, TYR_115, MET_122 , ARG_123, LEU_126, LEU_129, PRO_209, ALA_210, PHE_213, LEU_214, MET_283, ALA_286, ALA_287, PHE_289, ALA_290, LEU_355, ILE_356, MET_357, LEU_358, MET_359, ARG_360, PHE_415, GLY_416, ALA_417, VAL_419, HIS_420, LYS_421, CYS_422, ILE_423, GLY_424, TYR_456, HIS_457, THR_458, MET_459, VAL_461,	ASN_93, TYR_102, MET_105, PHE_109, ALA_114, TYR_115, ARG_123, LEU_126, LEU_129, LEU_133, LEU_207, MET_283, ALA_286, PHE_289, ALA_290, ARG_360, PHE_415 , VAL_419, HIS_420, LYS_421, CYS_422, ILE_423, MET_459,	PRO_98, TYR_102, MET_105, VAL_108, PHE_109, TYR_115, LEU_207, ALA_286, PHE_289, ALA_290, HIS_293, THR_294, LEU_355, MET_357, LEU_358, PHE_415, VAL_419, HIS_420, CYS_422, ILE_423, MET_459, VAL_460

LEU, leucine; ALA, alanine; GLY, glycine; THR, threonine; ILE, isoleucine; PRO, proline; PHE, phenylalanine; MET, methione; VAL, valine; ASN, asparagines; HIS, histidine; CYS, cysteine; ARG, arginine

contacts lie within the predicted binding sites, further supporting their relevance. Furthermore, the MD simulations revealed additional amino acid residues interacting with the ligands compared to the molecular docking results, indicating a broader binding mode and underscoring the dynamic nature of the binding site through additional contacts (Table IV). In contrast, the MD simulation of the control drug fluconazole with CYP51 showed a stable conformation, with minimal changes throughout the simulation. Hydrogen bonds with HIS 420 and CYS 422 were maintained for 95 per cent and 18 per cent of the simulation, indicating a more robust and consistent binding pattern. Fluconazole also formed more hydrophobic interactions (with 17 residues), suggesting a stable binding mode.

Posaconazole is a triazole antifungal with a complex structure, characterized by multiple chiral centers that enhance its potent inhibition of 14-alpha demethylase, making it highly effective in treating severe systemic infections. Its stereochemistry facilitates strong binding interactions, essential for its broad-spectrum activity[46,47]. In contrast, isavuconazole features a butan-2-ol backbone with various functional groups, including 1,2,4-triazol-1-yl, 2,5-difluorophenyl, and 4-(p-cyanophenyl)-1,3-thiazol-2-yl groups. These structural components enable it to disrupt cell membranes by reducing ergosterol levels[48,49]. Several studies have explored the use of different azole drugs to treat leishmaniasis. A study conducted by Shakya *et al*[50] in 2011, showcasing the combined use of ketoconazole and miltefosine with the immunomodulator picroliv against visceral leishmaniasis, suggested the potency of ketoconazole in combination therapy in treating leishmaniasis. Similarly, other studies have employed the use of fluconazole and itraconazole to target cutaneous leishmaniasis caused by *L. major*[51,52]. Our study suggested posaconazole and isavuconazole against the CYP51 enzyme of *L. major*. Posaconazole and isavuconazole, being broad-spectrum triazoles with enhanced bioavailability, possess a notable advantage[53,54]. *In vitro* study demonstrated that posaconazole and isavuconazole effectively inhibited the growth of *L. major* promastigotes, with respective IC_{50} values of 2.062±0.89 µg/ml and 1.202±0.65 µg/ml, respectively, suggesting their efficacy as anti-leishmanial agents.

In the present study, we observed that both posaconazole and isavuconazole act against the CYP51 enzyme of *L. major*. This was demonstrated by molecular docking and MD simulation studies. Additionally, an *in vitro* study using *L. major* strains suggested that both drugs can effectively kill the parasite's promastigote form. Therefore, these two drugs can potentially be repurposed for the treatment of cutaneous leishmaniasis.

However, there are several limitations to our study. Firstly, while the *in vitro* results are promising, the experiments were conducted only on the promastigote form of *L. major*, and the effects on the clinically relevant amastigote form remain to be determined. Additionally, although molecular docking studies suggest that these drugs target the CYP51 enzyme, further validation is required to confirm specific enzyme interactions in the parasite. To address these limitations, future research should focus on testing the efficacy of both drugs against the amastigote form of *L. major* in *in vivo* models. Additionally, conducting animal experiments would be essential to assess pharmacokinetics, toxicity, and drug efficacy in a living organism. Moreover, membrane-bound MD simulations in future studies could provide deeper insights into drug permeability and efficacy within a more physiologically relevant context. Finally, based on the individual efficacy of these drugs, future studies should investigate their synergistic potential to enhance therapeutic outcomes.

Use of Artificial Intelligence (AI)-Assisted Technology for manuscript preparation: The authors confirm that there was no use of AI-assisted technology for assisting in the writing of the manuscript and no images were manipulated using AI.

References

1. Mann S, Frasca K, Scherrer S, Henao-Martínez AF, Newman S, Ramanan P, *et al*. A Review of Leishmaniasis: Current knowledge and future directions. *Curr Trop Med Rep* 2021; *8* : 121-32.

2. Yadav P, Azam M, Ramesh V, Singh R. Unusual observations in Leishmaniasis-An Overview. *Pathogens* 2023; *12* : 297.

3. Costa CHN, Chang KP, Costa DL, Cunha FVM. From infection to death: An overview of the pathogenesis of Visceral Leishmaniasis. *Pathogens* 2023; *12* : 969.

4. Wamai RG, Kahn J, McGloin J, Ziaggi G. Visceral leishmaniasis: A global overview. *J Glob Health Sci* 2020; *2*: e3.

5. David CV, Craft N. Cutaneous and mucocutaneous leishmaniasis. *Dermatol Ther* 2009; *22* : 491-502.

6. Garrido-Jareño M, Sahuquillo-Torralba A, Chouman-Arcas R, Castro-Hernández I, Molina-Moreno JM, Llavador-Ros M, *et al*. Cutaneous and mucocutaneous leishmaniasis: Experience of a Mediterranean hospital. *Parasit Vectors* 2020; *13* : 24.

7. World Health Organization. *Leishmaniasis*. Available from: *https://www.who.int/news-room/fact-sheets/detail/leishmaniasis*, accessed on February 21, 2024.

8. Rai S, Bhaskar, Goel SK, Nath Dwivedi U, Sundar S, Goyal N. Role of efflux pumps and intracellular thiols in natural antimony resistant isolates of Leishmania donovani. *PLoS One* 2013; *8* : e74862.

9. Boozhmehrani MJ, Eslami G, Khamesipour A, Jafari AA, Vakili M, Hosseini SS, *et al*. The role of ATP-binding cassette transporter genes expression in treatment failure cutaneous leishmaniasis. *AMB Express* 2022; *12* : 78.

10. Fekrisoofiabadi M, Fekri M, Moradabadi A, Vahidi R, Khaleghi M, Ram M, *et al*. Evaluation of MDR1 and MRPA genes expression in different types of dry cutaneous leishmaniasis. *BMC Res Notes* 2019; *12* : 803.

11. Espada CR, Magalhães RM, Cruz MC, Machado PR, Schriefer A, Carvalho EM, *et al*. Investigation of the pathways related to intrinsic miltefosine tolerance in Leishmania (Viannia) braziliensis clinical isolates reveals differences in drug uptake. *Int J Parasitol Drugs Drug Resist* 2019; *11* : 139-47.

12. Vacchina P, Norris-Mullins B, Abengózar MA, Viamontes CG, Sarro J, Stephens MT, *et al*. Genomic Appraisal of the multifactorial basis for in vitro acquisition of miltefosine resistance in Leishmania donovani. *Antimicrob Agents Chemother* 2016; *60* : 4089-100.

13. Pountain AW, Weidt SK, Regnault C, Bates PA, Donachie AM, Dickens NJ, *et al*. Genomic instability at the locus of sterol C24-methyltransferase promotes amphotericin B resistance in Leishmania parasites. *PLoS Negl Trop Dis* 2019; *13* : e0007052.

14. Mwenechanya R, Kovářová J, Dickens NJ, Mudaliar M, Herzyk P, Vincent IM, *et al*. Sterol 14α-demethylase mutation leads to amphotericin B resistance in Leishmania mexicana. *PLoS Negl Trop Dis* 2017; *11* : e0005649.

15. Alpizar-Sosa EA, Ithnin NRB, Wei W, Pountain AW, Weidt SK, Donachie AM, *et al*. Amphotericin B resistance in Leishmania mexicana: Alterations to sterol metabolism and oxidative stress response. *PLoS Negl Trop Dis* 2022; *16* : e0010779.

16. Mansuri R, Singh J, Diwan A. An insight into the current perspective and potential drug targets for Visceral Leishmaniasis (VL). *Curr Drug Targets* 2020; *21* : 1105-29.

17. Dinesh N, Pallerla DS, Kaur PK, Kishore Babu N, Singh S. Exploring Leishmania donovani 3-hydroxy-3-methylglutaryl coenzyme A reductase (HMGR) as a potential drug target by biochemical, biophysical and inhibition studies. *Microb Pathog* 2014; *66* : 14-23.

18. Jain S, Sahu U, Kumar A, Khare P. Metabolic pathways of Leishmania Parasite: Source of pertinent drug targets and potent drug candidates. *Pharmaceutics* 2022; *14* : 1590.

19. Sharma VK, Bharatam PV. Identification of selective inhibitors of Ld DHFR Enzyme using pharmacoinformatic methods. *J Comput Biol* 2021; *28* : 43-59.

20. Herrmann FC, Sivakumar N, Jose J, Costi MP, Pozzi C, Schmidt TJ. In silico identification and in vitro evaluation of natural inhibitors of leishmania major Pteridine Reductase I. *Molecules* 2017; *22* : 2166.

21. Vishwakarma P, Parmar N, Chandrakar P, Sharma T, Kathuria M, Agnihotri PK, *et al*. Ammonium trichloro [1,2-ethanediolato-O,O']-tellurate cures experimental visceral leishmaniasis by redox modulation of Leishmania donovani trypanothione reductase and inhibiting host integrin linked PI3K/Akt pathway. *Cell Mol Life Sci* 2018; *75* : 563-88.

22. Singh S, Kumari E, Bhardwaj R, Kumar R, Dubey VK. Molecular events leading to death of Leishmania donovani under spermidine starvation after hypericin treatment. *Chem Biol Drug Des* 2017; *90* : 962-71.

23. Singh J, Srivastava A, Jha P, Sinha KK, Kundu B. L-Asparaginase as a new molecular target against leishmaniasis: Insights into the mechanism of action and structure-based inhibitor design. *Mol Biosyst* 2015; *11* : 1887-96.

24. McCall LI, El Aroussi A, Choi JY, Vieira DF, De Muylder G, Johnston JB, *et al*. Targeting ergosterol biosynthesis in Leishmania donovani: Essentiality of sterol 14 alpha-demethylase. *PLoS Negl Trop Dis* 2015; *9* : e0003588.

25. da Silva Santos-Júnior PF, Schmitt M, de Araújo-Júnior JX, da Silva-Júnior EF. Sterol 14α-demethylase from trypanosomatidae parasites as a promising target for designing new antiparasitic agents. *Curr Top Med Chem* 2021; *21* : 1900-21.

26. Sayers EW, Bolton EE, Brister JR, Canese K, Chan J, Comeau DC, *et al*. Database resources of the national center for biotechnology information. *Nucleic Acids Res* 2022; *50* : D20-D26.

27. Berman HM, Westbrook J, Feng Z, Gilliland G, Bhat TN, Weissig H, *et al*. The protein data bank. *Nucleic Acids Res* 2000; *28* : 235-42.

28. UniProt Consortium. UniProt: The universal protein knowledgebase in 2021. *Nucleic Acids Res* 2021; *49* : D480-9.

29. Waterhouse A, Bertoni M, Bienert S, Studer G, Tauriello G, Gumienny R, *et al*. SWISS-MODEL: Homology modelling of protein structures and complexes. *Nucleic Acids Res* 2018; *46* : W296-W303.

30. Laskowski RA, Rullmannn JA, MacArthur MW, Kaptein R, Thornton JM. AQUA and PROCHECK-NMR: Programs for checking the quality of protein structures solved by NMR. *J Biomol NMR* 1996; *8* : 477-86.

31. Accelrys Inc. Discovery Studio Visualizer (Version 21.1.0). Dassault Systèmes, 2022. Available from: *https://discover.3ds. com/discovery-studio-visualizer*, accessed on November 29, 2022.

32. Jendele L, Krivak R, Skoda P, Novotny M, Hoksza D. PrankWeb: A web server for ligand binding site prediction and visualization. *Nucleic Acids Res* 2019; *47* : W345-9.

33. Konc J, Janežič D. ProBiS-ligands: A web server for prediction of ligands by examination of protein binding sites. *Nucleic Acids Res* 2014; *42* : W215-20.

34. Wu Q, Peng Z, Zhang Y, Yang J. COACH-D: Improved protein-ligand binding sites prediction with refined ligand-binding poses through molecular docking. *Nucleic Acids Res* 2018; *46* : W438-42.

35. Irwin JJ, Sterling T, Mysinger MM, Bolstad ES, Coleman RG. ZINC: A free tool to discover chemistry for biology. *J Chem Inf Model* 2012; *52* : 1757-68.

36. O', Boyle NM, Banck M, James CA, Morley C, Vandermeersch T, *et al*. Open Babel: An open chemical toolbox. *J Cheminform* 2011; *3* : 33.

37. Dallakyan S, Olson AJ. Small-molecule library screening by docking with PyRx. *Methods Mol Biol* 2015; *1263* : 243-50.

38. Morris GM, Huey R, Lindstrom W, Sanner MF, Belew RK, Goodsell DS, *et al*. AutoDock4 and AutoDockTools4: Automated docking with selective receptor flexibility. *J Comput Chem* 2009; *30* : 2785-91.

39. Bharadwaj S, Lee KE, Dwivedi VD, Kang SG. Computational insights into tetracyclines as inhibitors against SARS-CoV-2 Mpro via combinatorial molecular simulation calculations. *Life Sci* 2020; *257* : 118080.

40. Umar HI, Ajayi AT, Mukerjee N, Aborode AT, Hasan MM, Maitra S, *et al*. Discovery of Novel hsp27 inhibitors as prospective anti-cancer agents utilizing computer-assisted therapeutic discovery approaches. *Cells* 2022; *11* : 2412.

41. Joshi J, Bandral C, Manchanda RK, Khurana A, Nayak D, Kaur S. Evidence for reversal of immunosuppression by homeopathic medicine to a predominant Th1-type immune response in BALB/c mice infected with *Leishmania donovani*. *Homeopathy* 2022; *111* : 31-41.

42. Kyari S. Epidemiology of Leishmaniasis. In: Almeida-Souza F, Cardoso F de O, Abreu-Silva AL, Calabrese K da S, editors. *Leishmania parasites-epidemiology, immunopathology and hosts*. London, UK: IntechOpen. 2024.

43. Briones Nieva CA, Cid AG, Romero AI, García-Bustos MF, Villegas M, Bermúdez JM. An appraisal of the scientific current situation and new perspectives in the treatment of cutaneous leishmaniasis. *Acta Trop* 2021; *221* : 105988.

44. McCall LI, El Aroussi A, Choi JY, Vieira DF, De Muylder G, Johnston JB, *et al*. Targeting Ergosterol biosynthesis in Leishmania donovani: Essentiality of sterol 14 alpha-demethylase. *PLoS Negl Trop Dis* 2015; *9* : e0003588.

45. Xu W, Hsu FF, Baykal E, Huang J, Zhang K. Sterol biosynthesis is required for heat resistance but not extracellular survival in leishmania. *PLoS Pathog* 2014; *10* : e1004427.

46. Lipp HP. Clinical pharmacodynamics and pharmacokinetics of the antifungal extended-spectrum triazole posaconazole: An overview. *Br J Clin Pharmacol* 2010; *70* : 471-80.

47. Chen L, Krekels EHJ, Verweij PE, Buil JB, Knibbe CAJ, Brüggemann RJM. Pharmacokinetics and Pharmacodynamics of Posaconazole. *Drugs* 2020; *80* : 671-95.

48. Lewis JS, Wiederhold NP, Hakki M, Thompson GR. New perspectives on antimicrobial agents: Isavuconazole. *Antimicrob Agents Chemother* 2022; *66* : e0017722.

49. Kim S, Chen J, Cheng T, Gindulyte A, He J, He S, *et al*. PubChem 2023 update. *Nucleic Acids Res* 2023; *51* : D1373-80.

50. Paniz Mondolfi AE, Stavropoulos C, Gelanew T, Loucas E, Perez Alvarez AM, Benaim G, *et al*. Successful treatment of Old World cutaneous leishmaniasis caused by Leishmania infantum with posaconazole. *Antimicrob Agents Chemother* 2011; *55* : 1774-6.

51. Alrajhi AA, Ibrahim EA, De Vol EB, Khairat M, Faris RM, Maguire JH. Fluconazole for the treatment of cutaneous leishmaniasis caused by Leishmania major. *N Engl J Med* 2002; *346* : 891-5.

52. Nassiri-Kashani M, Firooz A, Khamesipour A, Mojtahed F, Nilforoushzadeh M, Hejazi H, *et al*. A randomized, double-blind, placebo-controlled clinical trial of itraconazole in the treatment of cutaneous leishmaniasis. *J Eur Acad Dermatol Venereol* 2005; *19* : 80-3.

53. Zhang T, Shen Y, Feng S. Clinical research advances of isavuconazole in the treatment of invasive fungal diseases. *Front Cell Infect Microbiol* 2022; *12* : 1049959.

54. Gupta AK, Talukder M, Venkataraman M. Review of the alternative therapies for onychomycosis and superficial fungal infections: Posaconazole, fosravuconazole, voriconazole, oteseconazole. *Int J Dermatol* 2022; *61* : 1431-41.

For correspondence: Dr Rakesh Sehgal, Aarupadai Veedu Medical College & Hospital, Kirumampakkam, Puducherry 607 402, India
e-mail: sehgalpgi@gmail.com